AAS 25-115

CURVE-BASED AXES FOR SPECIFYING MANEUVERS IN A MULTI-BODY SYSTEM

Natasha Bosanac* **and Giuliana Miceli†**

Generating a thrust-enabled spacecraft trajectory in a multi-body system requires specifying the evolution of the thrust vector. A well-known basis vector set for specifying a thrust direction is the velocity-normal-conormal axes. Although these axes support heuristic maneuver design, they require specification of a reference point. As a trajectory passes through various regions of a multi-body system, these axes may lose physical meaning or require an evolving reference point. Inspired by these challenges, this paper examines curve-based, moving frames as an analog to the velocity-normal-conormal axes in a multi-body system, with a focus on the Frenet frame and rotation-minimizing frames.

INTRODUCTION

An increasing number of spacecraft are expected to operate with continuous thrust propulsion systems in multi-body gravitational systems such as cislunar space. Designing complex trajectories for these spacecraft requires specifying both its path through the phase space and the control profile, i.e., the time evolution of the magnitude and direction, for the propulsion system. These control histories may be computed to satisfy optimality criteria, achieve objectives, or based on heuristics. When computing both the trajectory and control history, the thrust vector direction is usually specified using a set of basis vectors that is tailored to the application. Common examples of useful basis vectors for specifying a thrust vector include inertial axes, axes of a rotating or synodic frame defined using two primary bodies, or the velocity-normal-conormal (VNC) axes relative to a desired reference point and observer.

The VNC axes adapt to the shape of the path relative to a specified reference point and support the use of maneuvering heuristics. Originally derived from the two-body problem, thrusting in the velocity direction most efficiently increases spacecraft energy relative to a specified reference point whereas thrusting in the normal direction most efficiently changes the orbital angular momentum vector. However, in a multi-body system, a spacecraft may pass through various regions of the system and revolve about different reference points. Accordingly, the VNC axes can lose physical meaning when specified relative to a single reference point, pass through a singularity, or require changing the reference point over time.

*Assistant Professor, Colorado Center for Astrodynamics Research, Smead Department of Aerospace Engineering Sciences, University of Colorado Boulder, 3775 Discovery Drive, Boulder, CO 80303.

†Graduate Researcher, Colorado Center for Astrodynamics Research, Smead Department of Aerospace Engineering Sciences, University of Colorado Boulder, 3775 Discovery Drive, Boulder, CO, 80303.

Approved for public release; distribution is unlimited. Public Affairs release approval #AFRL-2024-7001. The views expressed are those of the author and do not reflect the official guidance or position of the United States Government, the Department of Defense, or of the United States Air Force.

This paper is motivated by the challenge of defining a generalizable set of basis vectors analogous to the VNC axes that adapts to the shape of a spacecraft trajectory in a multi-body system. Furthermore, the goal is for these axes to retain some useful heuristics for maneuvering with a continuous thrust propulsion system. To address these challenges, we leverage technical concepts from the fields of differential geometry and computer graphics.

The field of differential geometry has used a variety of adapted, moving frames that define a set of orthogonal, right-handed axes that evolve with the curvature of the path. One well-known, foundational frame is the Frenet frame that uses the curvature and osculating plane to mathematically calculate the axes. One axis aligns with the tangent to the curve whereas another points towards the center of curvature in the osculating plane. However, these axes can suffer from discontinuities when the curvature passes through zero. In computer graphics and robotics, rotation-minimizing frames have been used to identify moving, adapted frames that, in some cases, do not suffer from discontinuities or exhibit a slower rate of rotation. These axes are constructed to use the tangent vector along with two vectors that lie in the plane normal to the tangent vector. These vectors can be parallel transported or exhibit smaller orientation changes.

This paper focuses on calculating two curve-based axes from the position, velocity, and acceleration vectors along a spacecraft trajectory in a multi-body system. These axes include the Frenet frame and a rotation-minimizing frame. Specifically, this paper focuses on motion in the Earth-Moon circular restricted three-body problem (CR3BP). Several example trajectories are calculated to span motions with distinct geometries, passing through distinct regions of the system. Along each trajectory, axes of these frames are calculated and the evolution of the basis vector sets are examined. This analysis also includes their direction relative to the physically interpretable $\pm\hat{B}_F$ and $\pm\hat{N}_F$ directions from the Frenet frame, the time rate of change of these basis vectors, and their behavior near points where the curvature passes through zero.

BACKGROUND

Dynamical Model

For this proof of concept, spacecraft trajectories are generated in a low-fidelity model of cislunar space known as the Earth-Moon circular restricted three-body problem (CR3BP). This model captures the point mass gravitational influence of the Earth and Moon as they follow circular orbits [1]. The spacecraft is assumed to possess a comparatively negligible mass.

In the CR3BP, trajectories are typically generated and analyzed in the Earth-Moon rotating frame using nondimensional coordinates. In the rotating frame, the origin is selected as the Earth-Moon barycenter and the axes are defined as follows: $\hat{x}$ points from the Earth to the Moon, $\hat{z}$ points in the direction of the Earth-Moon orbital angular momentum vector, and $\hat{y}$ completes the orthogonal, right-handed triad [1]. In addition, mass, length, and time quantities are nondimensionalized to ensure that the total system mass, primary orbit radius, and mean motion of the Earth-Moon system are all equal to unity [1, 2].

These definitions enable formulation of the equations of motion governing the spacecraft in the CR3BP. The nondimensional state of the spacecraft is denoted in the rotating frame as $\bar{x} = [x, y, z, \dot{x}, \dot{y}, \dot{z}]^T$ with $\bar{r} = [x, y, z]^T$ and $\bar{v} = [\dot{x}, \dot{y}, \dot{z}]^T$; in these definitions, $\dot{(.)}$ denotes a time derivative with an observer in the rotating frame. The equations of motion are then written as

$$\ddot{x} - 2\dot{y} = \frac{\partial U^*}{\partial x}, \qquad \ddot{y} + 2\dot{x} = \frac{\partial U^*}{\partial y}, \qquad \ddot{z} = \frac{\partial U^*}{\partial z} \tag{1}$$

where the pseudo-potential function is defined as

$$U^* = \frac{x^2 + y^2}{2} + \frac{1-\mu}{r_1} + \frac{\mu}{r_2} \tag{2}$$

In these expressions, the mass ratio μ is the ratio of the Moon's mass to the total mass of the system, $r_1 = \sqrt{(x+\mu)^2 + y^2 + z^2}$, and $r_2 = \sqrt{(x-1+\mu)^2 + y^2 + z^2}$ [1]. These equations of motion produce an autonomous dynamical system in the rotating frame. The Jacobi constant is a constant of motion that exists in the rotating frame and is equal to

$$C_J = 2U^* - \dot{x}^2 - \dot{y}^2 - \dot{z}^2 \tag{3}$$

Due to its form, this quantity is comparable to a spacecraft energy: as C_J increases, the spacecraft energy decreases.

Velocity-Normal-Conormal Axes

The Velocity-Normal-Conormal (VNC) axes are derived from the two-body problem and supply heuristics for efficiently maneuvering. These VNC axes are defined relative to a reference point such as a celestial body and a selected observer frame. Given a reference body with position and velocity vectors $\bar{r}_P$ and $\bar{v}_P^O$, the spacecraft's relative position and velocity vectors are denoted as $\bar{r}_{P,sc} = \bar{r} - \bar{r}_P$ and $\bar{v}_{P,sc}^O = \bar{v}^O - \bar{v}_P^O$. In these expressions, the superscript O identifies a specified observer frame, e.g., an inertial or rotating frame; commonly, the inertial frame is used due to the connection to the two-body problem. Using these relative state components, the VNC axes are mathematically calculated as

$$\hat{V}_{VNC} = \frac{\bar{v}_{P,sc}^O}{||\bar{v}_{P,sc}^O||} \qquad \hat{N}_{VNC} = \frac{\bar{r}_{P,sc} \times \bar{v}_{P,sc}^O}{||\bar{r}_{P,sc} \times \bar{v}_{P,sc}^O||} \qquad \hat{C}_{VNC} = \hat{V}_{VNC} \times \hat{N}_{VNC} \tag{4}$$

Based on this definition, thrusting in the $\pm\hat{V}_{VNC}$ direction most efficiently increases or decreases the spacecraft energy relative to the primary. Furthermore, thrusting in the $\pm\hat{N}_{VNC}$ direction most efficiently changes the orbit normal direction.

When applied to a multi-body system, the VNC axes may lose physical meaning and experience a singularity. Specifically, as a path revolves around reference points other than the selected celestial body, the relative position and velocity vectors can become parallel or anti-parallel, leading to an undefined $\hat{N}_{VNC}$ vector. Furthermore, the $\hat{C}_{VNC}$ and $\hat{N}_{VNC}$ become less meaningful when the path revolves around a different region of the phase space than the location of the reference point.

Curvature

In differential geometry, many curve-based frames rely on curvature concepts. Consider a spatial trajectory with position, velocity, and acceleration vectors that are labeled $\bar{r}(t) = [x(t), y(t), z(t)]^T$, $\bar{v}(t) = [\dot{x}(t), \dot{y}(t), \dot{z}(t)]^T$, and $\bar{a}(t) = [\ddot{x}(t), \ddot{y}(t), \ddot{z}(t)]^T$, respectively. When the trajectory is generated over a time interval $t \in [t_0, t_f]$, it traces out an arclength s that is equal to [3]

$$s = \int_{t_0}^{t_f} ds = \int_{t_0}^{t_f} \sqrt{\dot{x}^2 + \dot{y}^2 + \dot{z}^2} dt \tag{5}$$

As the spacecraft follows this path, this quantity increases over time.

At any state along the trajectory, the trajectory may be bending and twisting. The curvature, $\kappa(t)$ captures the rate of change of the velocity unit vector, i.e., the tangent to the curve, with respect to arclength [4]. As a result, the curvature captures the extent to which the path deviates from a straight line in the osculating plane. Note the osculating plane is the plane formed by three sequential points as their separation approaches an infinitesimally small value [4]. Mathematically, this nonnegative quantity is calculated as [4]

$$\kappa(t) = \frac{||\dot{\bar{r}}(t) \times \ddot{\bar{r}}(t)||}{||\dot{\bar{r}}(t)||^3} = \frac{\sqrt{(\ddot{z}\dot{y} - \ddot{y}\dot{z})^2 + (\ddot{x}\dot{z} - \ddot{z}\dot{x})^2 + (\ddot{y}\dot{x} - \ddot{x}\dot{y})^2}}{(\dot{x}^2 + \dot{y}^2 + \dot{z}^2)^{3/2}} \tag{6}$$

This curvature is typically unsigned when describing spatial paths and is inversely proportional to the radius of curvature. However, the curvature possesses a singularity when the speed is equal to zero. The torsion $\tau(t)$ captures the rate of change of the orientation of the osculating plane. When $\kappa(t) \neq 0$, torsion is mathematically calculated as

$$\tau(t) = \frac{\bar{r}(t)\dot{\bar{r}}(t)\ddot{\bar{r}}(t)}{||\dot{\bar{r}}(t) \times \ddot{\bar{r}}(t)||^2} = \frac{\dddot{x}(\dot{y}\ddot{z} - \ddot{y}\dot{z}) + \dddot{y}(\ddot{x}\dot{z} - \dot{x}\ddot{z}) + \dddot{z}(\dot{x}\ddot{y} - \ddot{x}\dot{y})}{(\dot{y}\ddot{z} - \ddot{y}\dot{z})^2 + (\dot{x}\ddot{z} - \ddot{x}\dot{z})^2 + (\dot{x}\ddot{y} - \ddot{x}\dot{y})^2} \tag{7}$$

with the sign reflecting the direction in which the osculating plane orientation is changing [4]. This quantity possesses a singularity when the curvature is zero, i.e., when there is an inflection point along the path. In that case, the torsion can be calculated as

$$\tau(t) = \frac{1}{2v^3\dot{\kappa}} \left(\frac{d^4\bar{r}(t)}{dt^4} \cdot \hat{b}(t) \right) \tag{8}$$

where $\hat{b}$ is the binormal vector, defined in the following section [4].

Curve-Based Frames

Curve-based frames have been presented and used in differential geometry and computer graphics. These axes depend only on the shape of the curve, not the location of the path in the configuration space [5]. There are multiple options for defining meaningful curve-based axes, with each approach producing distinct characteristics in the existence and evolution of these axes.

Frenet Frame The axes of the Frenet frame are derived directly from the curvature vector and use the time derivatives of the position vector. Specifically, the three axes are defined as follows: $\hat{T}_F$ is tangent to the path in the direction of motion; the principal normal $\hat{N}_F$ is directed towards the center of curvature and lies in the osculating plane; and the binormal vector $\hat{B}_F$ is normal to the osculating plane and completes the orthogonal, right-handed triad [3]. Accordingly, the normal plane is spanned by $\hat{N}_F$ and $\hat{B}_F$. Note, however, that despite the terminology, the $\hat{B}_F$ vector is most similar to the normal vector $\hat{N}_{VNC}$ of the VNC axes. When the curvature is nonzero, i.e., $\kappa \neq 0$, these three basis vectors are computed as [3]

$$\hat{T}_F = \frac{\bar{v}}{|\bar{v}|} = \frac{\dot{\bar{r}}}{|\dot{\bar{r}}|} \qquad \hat{N}_F = \hat{B}_F \times \hat{T}_F \qquad \hat{B}_F = \frac{\bar{v} \times \bar{a}}{|\bar{v} \times \bar{a}|} = \frac{\dot{\bar{r}} \times \ddot{\bar{r}}}{|\dot{\bar{r}} \times \ddot{\bar{r}}|} \tag{9}$$

As these basis vectors are calculated along a trajectory, they evolve with the curvature and direction of motion. However, as a trajectory evolves from convex to concave, passing through a zero curvature or inflection point, the binormal and normal axes, $\hat{B}_F$ and $\hat{N}_F$, are instantaneously undefined.

In that case, when the curvature is instantaneously zero but its first time derivative is nonzero, i.e., $\kappa = 0$ and $\dot{\kappa}(t) \neq 0$, the $\hat{N}_F$ and $\hat{B}_F$ vectors can be calculated as

$$\hat{N}_F = \frac{\dddot{\bar{r}}(t) - \ddot{v}\hat{T}_F}{v^2\dot{\kappa}} \qquad \hat{B}_F = \hat{T}_F \times \hat{N}_F \tag{10}$$

which is derived directly from the third time derivative of the position vector expressed in the axes of the Frenet frame, simplifying with $\kappa = 0$ [4]. On either side of this inflection point, these two vectors exhibit rapid changes in orientation, typically flipping direction. Accordingly, while the Frenet frame adapts to the curvature of the path, it may not supply slowly varying basis vectors.

Rotation-Minimizing Frames A rotation-minimizing frame (RMF) is defined such that two basis vectors do not instantaneously rotate about the remaining vector. It is common to use the same tangent vector $\hat{T}_R$ as the Frenet frame, calculated directly from the instantaneous tangent to the path [6]. Then, the plane normal to the tangent vector is used to define the remaining two basis vectors to form an orthogonal triad. Unlike the Frenet frame, however, the two remaining basis vectors are selected in a rotation-minimizing frame to ensure that there is no instantaneous rotation about the tangent vector [6]. For these rotation-minimizing frames with basis vectors $\hat{T}_R, \hat{M}_{1,R}, \hat{M}_{2,R}$, their evolution over the arclength of the trajectory is governed by the following expressions:

$$\frac{d\hat{T}_R}{ds} = \bar{\omega} \times \hat{T}_R \qquad \frac{d\hat{M}_{1,R}}{ds} = \bar{\omega} \times \hat{M}_{1,R} \qquad \frac{d\hat{M}_{2,R}}{ds} = \bar{\omega} \times \hat{M}_{2,R} \tag{11}$$

where $\bar{\omega}$ is the angular velocity that is selected as desired. There are multiple options for selecting this angular velocity vector, rendering rotation-minimizing frames non-unique. One common approach sets $\bar{\omega} \cdot \hat{T}_R = 0$.

Rotation-minimizing frames have been used in applications such as computer graphics and computer aided geometric design because they mitigate excessive rotation of the axes in the normal plane. Specifically, rotation-minimizing frames have been used to define smoothly varying camera paths, visualize streamlines, generate smooth shapes in computer graphics, and support path planning for robotic systems [6]. Furthermore, depending on the formulation, these axes may be defined even when $\kappa = 0$ at an inflection point in curvature. These types of frames can be computed in different ways, depending on the characteristics of the problem. For instance, difference choices in the $\bar{\omega}$ rotation vector and, therefore, the differential equations governing the evolution of the axes can result in RMFs with distinct characteristics.

Existing approaches to computing the basis vectors of a rotation-minimizing frame include numerical integration from an initial set, discrete approximation, and using a spine curve representation of the path [6]. A numerical integration approach focuses on 1) directly generating solutions to the differential equations defining the basis vectors or 2) integrating the total torsion τ_{tot} over the curve and rotating $\hat{B}_F$ and $\hat{N}_F$ accordingly [5] [7]. This approach supports calculating basis vectors at each instant of time during trajectory generation, but can sometimes suffer from singularities depending on the approach used to calculate the torsion. In a discrete approximation approach, samples $\bar{x}_i$ are taken from the curve $\bar{x}(s)$, with the basis vectors for a rotation-minimizing frame calculated at each subsequent point using a geometric approach such as the projection method or double reflection method [6]. Although these approaches are mathematically straightforward, they are usually used for post-processing rather than during trajectory generation. Spine curve approximation identifies simple curves with analytical solutions to the equations governing the rotation-minimizing frame that are similar in geometry to the spine curve of interest, taking these basis

vectors as approximations for the actual curve [8]. Of these approaches, this paper uses either direct computation or numerical integration to ensure that the axes can be computed during trajectory generation to support instantaneous calculation of the basis vectors.

One approach to formulating an RMF relies on the concept of parallel vector fields. Consider a curve $\bar{r}(s)$ as a function of arclength and a vector field $\bar{V}(s)$ that is normal to the tangent $\bar{T}(s)$ at a selected point. Then, the normal vector field $\bar{V}(s)$ is denoted as parallel to the curve $\bar{r}(s)$ if the derivative of the field is parallel to the curve, i.e., $\dot{\bar{V}}(s)||\bar{T}(s)$ [9]. In general, a vector field $\bar{V}(s)$ is parallel to a curve $\bar{r}(s)$ if its normal component is tangential to $\bar{r}(s)$ [9]. Given this definition, the curve $\bar{q}(s) = \bar{r}(s) + \bar{V}(s)$ is a parallel curve to $\bar{x}(s)$ [9]. Parallel vector fields are characterized by several properties, the following of which are most useful for computing RMFs [9]:

- $\bar{V}(s)$ turns just as much as necessary to remain normal.
- An initial normal vector $\bar{V}_0$ at a point $\bar{r}(s_0)$ generates a unique parallel field $\bar{V}(s)$ on $\bar{r}(s)$ such that $\bar{V}(s_0) = \bar{V}_0$.
- If normal vectors $\bar{V}_0$ and $\bar{U}_0$ generate parallel fields $\bar{V}(s)$ and $\bar{U}(s)$ respectively, the angle between the two parallel fields is constant along the curve, i.e. $\bar{V}(s) \cdot \bar{U}(s) = \bar{V}_0 \cdot \bar{U}_0$

These properties are useful for computing RMFs even in cases where the curvature is zero or when the trajectory experiences sudden changes in curvature.

The parallel transport approach offers one mechanism for calculating an RMF [9]. This frame leverages a set of axes such as those associated with the Frenet frame at an initial state $\bar{x}(s_0)$, i.e., $\hat{T}_{F,0}, \hat{N}_{F,0}, \hat{B}_{F,0}$. This initial set of axes are then parallel transported along the trajectory while maintaining its orthonormal properties. This approach ensures a smooth variation in the axes because the derivatives of the axes normal to $\bar{T}$ only depend on the tangent to the curve, not necessarily the curvature. Mathematically, the differential equations governing the three axes of the parallel transport frame are equal to

$$\begin{bmatrix} \dot{\bar{T}} \\ \dot{\bar{M}}_1 \\ \dot{\bar{M}}_2 \end{bmatrix} = v \begin{bmatrix} 0 & k_1 & k_2 \\ -k_1 & 0 & 0 \\ -k_2 & 0 & 0 \end{bmatrix} \begin{bmatrix} \bar{T} \\ \bar{M}_1 \\ \bar{M}_2 \end{bmatrix} \tag{12}$$

where k_1 and k_2 are related to the curvature and torsion as:

$$\kappa(t) = ||k_1 + k_2|| \qquad \theta(t) = \tan^{-1}\left(\frac{k_2}{k_1}\right) \qquad \tau(t) = -\frac{d\theta}{dt} \tag{13}$$

The parallel transport frame can be computed for any curve. This approach is described in Algorithm 1, following the approach presented by Hanson and Ma [9]. Note that when the direction of the tangent vector does not change, i.e., the curvature is zero, the frame at time i is repeated at time $i + 1$.

Along closed curves such as periodic trajectories in the CR3BP, this formulation of the parallel transport frame exhibits a noticeable issue. Specifically, the parallel transport frame will generally not return to its initial orientation, unless the total accumulated torsion along a curve sums up to zero. The difference between the axes at the initial and final states is equal to

$$\alpha = -\oint \tau(s) ds \bmod (2\pi) \tag{14}$$

Algorithm 1 Compute each normal axis of the parallel transport frame

Require: (a) $\bar{T}_i$ with $i = 1, ..., N$ where N is the length of the states along the curve; (b) initial normal vector $\bar{M}_{i,0}, \bar{M}_{i,0} \perp \bar{T}_0$.

for $i = 1 \rightarrow N - 1$ **do**
  $\bar{V}_{rot} = \bar{T}_i \times \bar{T}_{i+1}$
  if $||\bar{V}_{rot}|| = 0$ **then**
    $\bar{N}_{i+1} = \bar{N}_i$
  else
    $\theta = arcos(\bar{T}_i \cdot \bar{T}_{i+1})$;
    $\bar{N}_{i+1} = R(\bar{V}_{rot}, \theta) \cdot \bar{N}_i$; // where R is the Rodrigues' rotation formula
    $\bar{N}_{i+1} = \bar{N}_{i+1}/||\bar{N}_{i+1}||$;
    $\bar{B} = \bar{T}_{i+1} \times \bar{N}_{i+1}$;
  end if
end for

However, this issue can be straightforwardly addressed by incorporating the twisting of the osculating plane, i.e., the torsion, into the calculation of the basis vectors. This involves incorporating spin around the tangential axis $\bar{T}$ to account for the integrated torsion from the initial state to the current state. In this modification, the normal axis can be written as:

$$\bar{N}_i = R(\bar{T}_i, \alpha_i) \cdot \bar{N}_i \tag{15}$$

where $\alpha_i = -\int_{s_0}^{s} \tau ds'$. Adding the additional spin ensures the periodicity of the parallel transport frame. Of course, in this case, the frame is no longer rotation-minimizing and, instead, more closely resembles the Frenet frame. This frame computation also requires being able to calculate the torsion at every instant of time along a trajectory.

RESULTS AND DISCUSSION

Overview of Scenarios

To examine the utility of curve-based axes as an analog to the VNC axes, the basis vectors are computed across a variety of geometrically diverse paths. These paths are summarized in Table 1 via their truncated initial state and integration time. For each path, the following frames are computed and compared: 1) the Frenet axes, 2) the parallel transport axes, and 3) the parallel transport axes with an additional spin that captures the influence of torsion. Both parallel transport axes use the Frenet axes at the initial state to generate subsequent axes along the trajectory, as described in the previous section. In each case, the axes are visualized throughout this section. Then, for selected paths, the difference between the parallel transport axes and the Frenet axes is assessed as a mechanism to understand the value of these axes in maintaining meaningful geometrical information. For instance, because the binormal direction in the Frenet axes is perpendicular to the osculating plane, the $\hat{B}_F$ axis supplies insight into a plane that is comparable to an instantaneous orbit plane. Any parallel transport axes that remain close to $\hat{B}_F$ could potentially approximate this meaningful direction. In addition, the time rate of change of the axes is discretely approximated using a finite difference to assess how quickly the axes evolve in the rotating frame. Such information could inform their potential use in defining basis vectors for continuous thrust directions by reflecting the orientation changes required for the thruster.

Initial State	Propagation Time
L_1 Lyapunov	
$\vec{x}_0 = [0.797128380, 0, 0, 0.375358878, 0]^T$	$T = 3.42544586$
$3:1$ interior resonant orbit	
$\vec{x}_0 = [0.091959358, 0, 0, 0, 4.00167032, 0]^T$	$T = 6.36752650$
Distant retrograde orbit (DRO)	
$\vec{x}_0 = [0.88701149, 0, 0, 0, 0.47105175, 0]^T$	$T = 1.53421803$
L_1 vertical	
$\vec{x}_0 = [0.88800682, 0, 0, 0, -0.29586668, -0.94140818]^T$	$T = 6.14095571$
L_1 axial	
$\vec{x}_0 = [0.83121770, 0, 0, 0, 0.24086954, 0.36617079]^T$	$T = 4.04550860$
L_1 northern halo	
$\vec{x}_0 = [0.83203901, 0, 0.12603694, 0, 0.24012675, 0]^T$	$T = 2.78240791$
General Trajectory	
$\vec{x}_0 = [0.804, -0.076, 0.044, 0.04934439, 0.10310450, 0.01606438]^T$	$T = [3, 8, 10]$

Table 1. Initial conditions and propagation time for each sample trajectory

Planar Periodic Orbits

The curve-based axes of interest in this paper are computed for three planar periodic orbits. These axes are plotted in Figure 1 with the following color scheme: the magenta vector indicates the tangent vector, $\hat{T}_F = \hat{T}_R$; the green vector corresponds to the binormal direction $\hat{B}_F$ and one normal vector $\hat{M}_{R,1}$ in each set of parallel transport axes; and the blue vector corresponds to the normal direction $\hat{N}_F$ and one normal vector $\hat{M}_{R,2}$ in each set of parallel transport axes. In each figure, the Moon is displayed with a gray sphere and the equilibrium points are plotted with black diamonds.

For the DRO, the path revolves around the Moon with litte variation in the curvature and no curvature inflection points. As a result, the three curve-based axes are all aligned. Furthermore, the binormal vector $\hat{B}_F$ (green) points perpendicular to the single orbit plane, in the $-\hat{z}$ direction, consistent with the spacecraft's orbital angular momentum vector while traveling in retrograde motion. The normal vector $\hat{N}_F$ points radially inwards towards the center of curvature.

The L_1 Lyapunov orbit is an interesting example due to the presence of two zero curvature points. For the majority of the orbit, the binormal direction from the Frenet frame and one normal direction in the parallel transport frames are aligned and pointed in the $-\hat{z}$-direction, consistent with the spacecraft traveling in a retrograde direction around L_1. However, near the rightmost x-axis crossing and between the two curvature points, the $\hat{B}_F$ and $\hat{M}_{2,R}$ directions differ. In the Frenet frame,

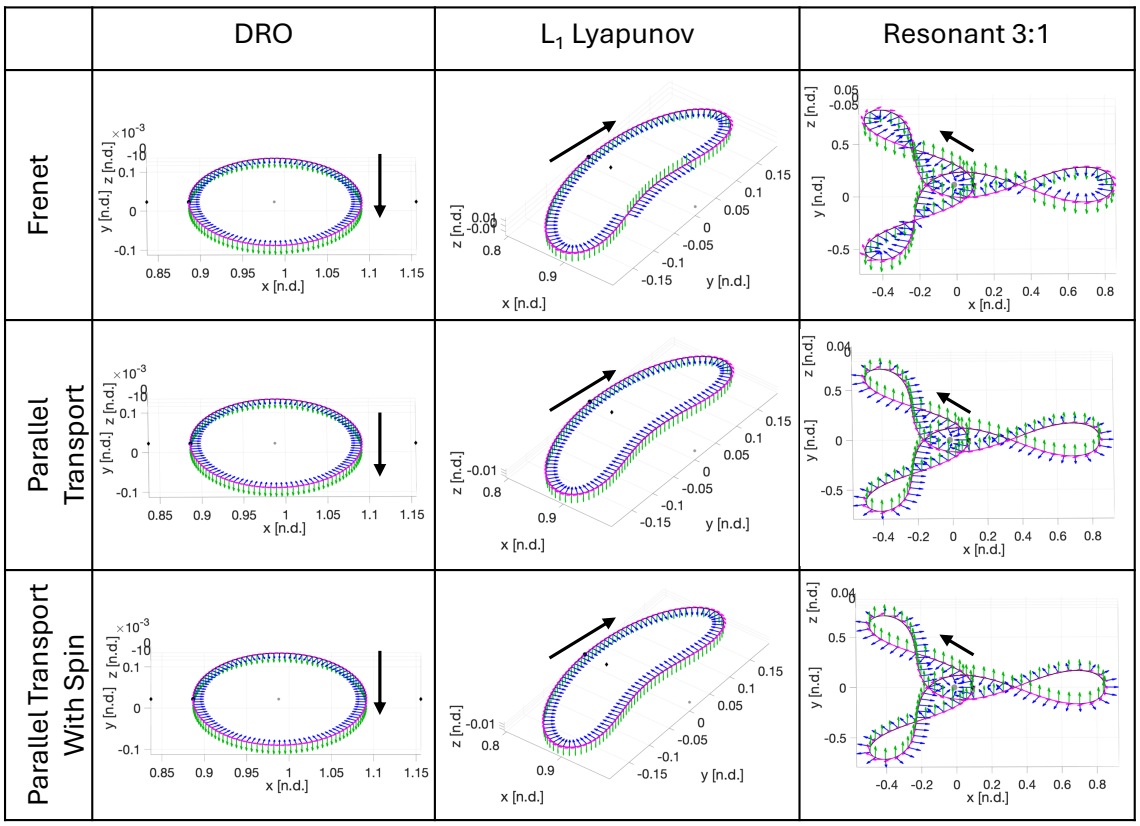

Figure 1. Examples of basis vectors computed along three planar periodic orbits using three distinct approaches. Basis vectors are colored as: tangent (magenta) and two vectors normal to tangent (green and blue). In the Frenet axes, green indicates the normal vector $\hat{N}_F$ and blue indicates the binormal vector $\hat{B}_F$.

the binormal direction flips as the path now possesses a center of curvature outside the orbit. However, for the two parallel transport axes, $\hat{M}_{2,R}$ does not flip direction and continues to point in the $-\hat{z}$-direction. Accordingly, for this planar orbit, the parallel transport approach offers a mechanism for calculating smoothly varying basis vectors with $\hat{M}_{2,R}$ always pointing normal to the orbit plane (in either the $+\hat{B}_F$ or $-\hat{B}_F$ direction), retaining the geometric insight afforded by the Frenet frame.

Along the 3:1 interior resonant orbit, the direction of motion relative to the Moon changes multiple times, rendering this example useful for analysis. The Frenet axes capture this change in the center of curvature, inside or outside of the orbit, as the green binormal vector $\hat{B}_F$ flips between the $+\hat{z}$ and $-\hat{z}$ axes and the green normal vector $\hat{N}_F$ flips between pointing inwards or outwards. In the parallel transport axes, $\hat{M}_{1,R}$ consistently points in the $+\hat{z}$ axis and $\hat{M}_{1,R}$ exhibits no discontinuities. For continuity, $\hat{M}_{1,R}$ sometimes points inwards or outwards. Of course, these directions depend on the selected initial state. If, however, the initial state was used to calculate Frenet axes that pointed in a different directions, $\hat{M}_{1,R}$ and $\hat{M}_{2,R}$ would point in the opposite directions to the plotted vectors.

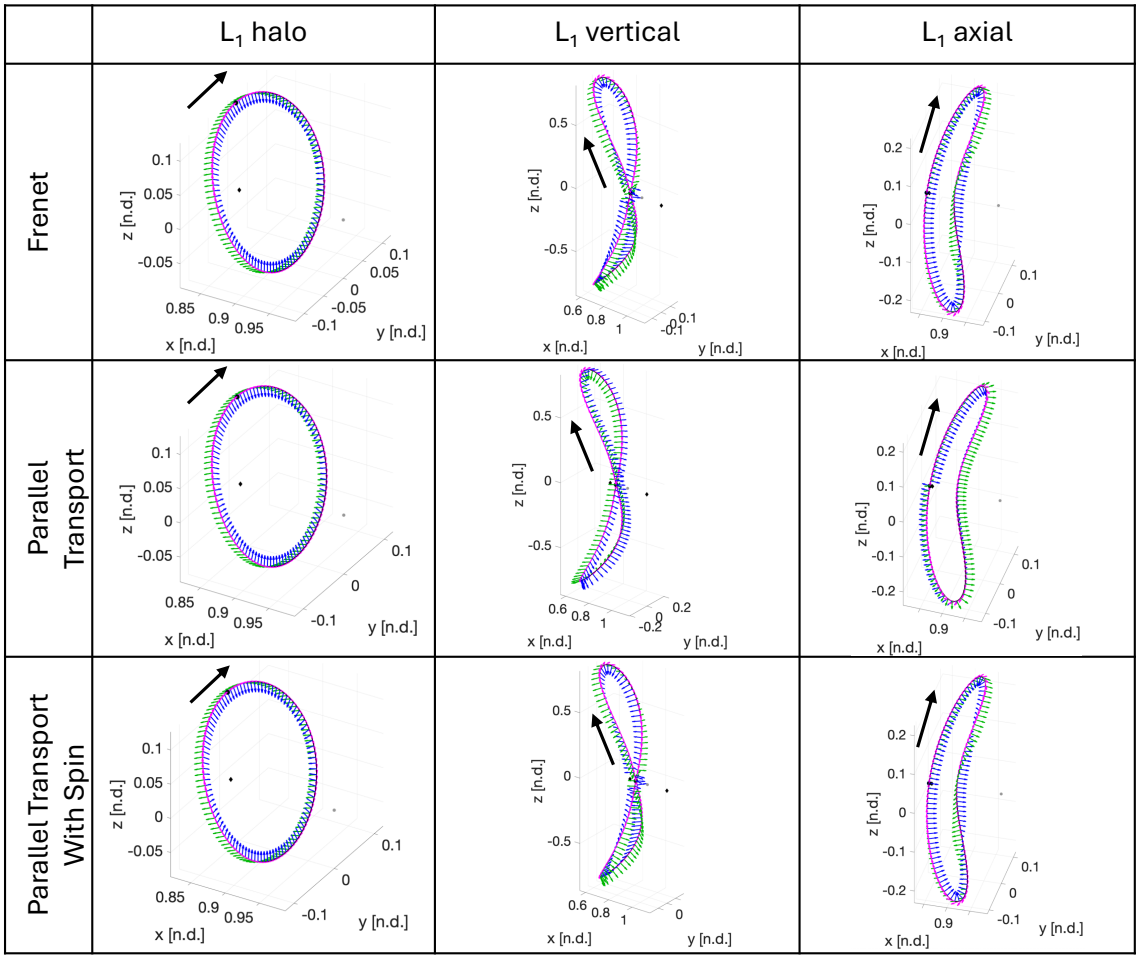

Figure 2. Examples of basis vectors computed along three spatial periodic orbits using three distinct approaches. Basis vectors are colored as: tangent (magenta) and two vectors normal to tangent (green and blue). In the Frenet axes, green indicates the normal vector $\hat{N}_F$ and blue indicates the binormal vector $\hat{B}_F$.

Spatial Periodic Orbits

Because spatial paths experience a twist in their osculating plane due to torsion, the difference between the three frames becomes more apparent when applied to spatial periodic orbits. Three orbits near L_1 are selected, with increasingly complex geometries. In each case, the axes at selected locations are plotted in Figure 2. Then, Figure 3 displays the angular difference between the axes from the two parallel transport axes and the Frenet axes for the L_1 vertical and L_1 axial orbits. Finally, Figure 4 displays the approximate time rate of change for the $\hat{T}$ and one vector that is calculated using the binormal vector $\hat{B}_F$ from the Frenet axes.

The L_1 northern halo orbit exhibits little change in the orientation of the osculating plane. Accordingly, the three axes produce identical basis vectors. In each case, the axes are also periodic, returning to the same orientation after one period. In the case of the Frenet frame, this is expected due to the use of direct analytical expressions. However, this is an interesting observation for the parallel transport approach. In each case the $\hat{B}_F$ and $\hat{M}_{2,R}$ axes all possess a negative z-component,

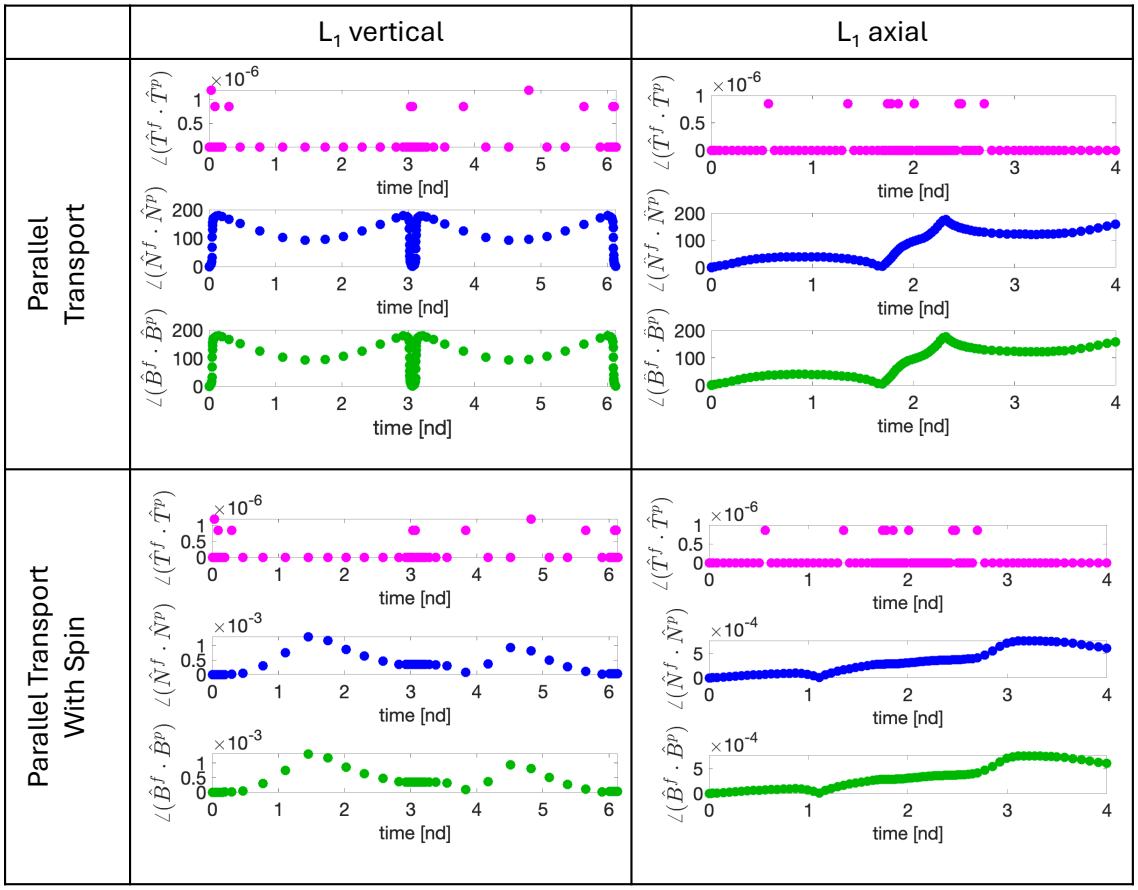

Figure 3. Comparison between the directions of the basis vectors computed in each parallel transport approach and the Frenet axes for two spatial orbits.

consistent with a clockwise rotation about an evolving center of curvature. Meanwhile, the $\hat{N}_F$ and $\hat{M}_{1,R}$ axes point inwards towards the center of curvature.

The L_1 vertical orbit is an interesting example due to its substantial change in the orientation of the osculating plane and symmetry about the xy-plane. In this case, the $\hat{B}_F$ binormal vector exhibits substantial changes in direction. A similar observation applies to the parallel transport approach that incorporates additional spin to mimic the torsion that is inherently captured in the Frenet axes. In fact, the two sets of normal vectors, $\hat{B}_F$ and $\hat{M}_{2,R}$ as well as $\hat{N}_F$ and $\hat{M}_{1,R}$, are closely aligned. In both frames, the tangent vector possess an angular rate of change on the order of 10^{-4} deg/s. The vectors that are normal to the tangent vector, however, experience substantial changes near the crossing of the xy-plane every half period; this angular rate of change reaches almost 0.05 deg/s, which is approximately 3 deg/min, but is much lower elsewhere. For the parallel transport approach that does not capture torsion, there is little rotation of $\hat{M}_{1,R}$ and $\hat{M}_{2,R}$ as the axes do not evolve with the changing orientation of the osculating plane. Furthermore, the angular rate of change of all three axes is on the order of 10^{-4} deg/s. As a result, the two vectors $\hat{M}_{1,R}$ and $\hat{M}_{2,R}$ deviate substantially from their original $\hat{N}_F$ and $\hat{B}_F$ vectors at the initial condition. Once the spacecraft is sufficiently out of the xy-plane, this deviation varies between approximately 90 and 180 degrees.

Finally, the L_1 axial orbit offers an interesting example as the curvatures becomes quite small

at two locations near the rightmost crossing of the xz-plane; note, however, that it does not equal exactly zero at any location. In this case, the Frenet axes substantially change direction around these low curvature regions, consistent with the center of curvature flipping. The parallel transport frame with torsion incorporated mimics this behavior. However, in the parallel transport frame with no torsion corrections, the axes vary smoothly but slowly drift away from the Frenet axes. Furthermore, these axes are not periodic after one period. Rather, they are the pointed in opposite directions, similar to traveling out the surface of a Möbius strip. Parallel transport frames are typically described

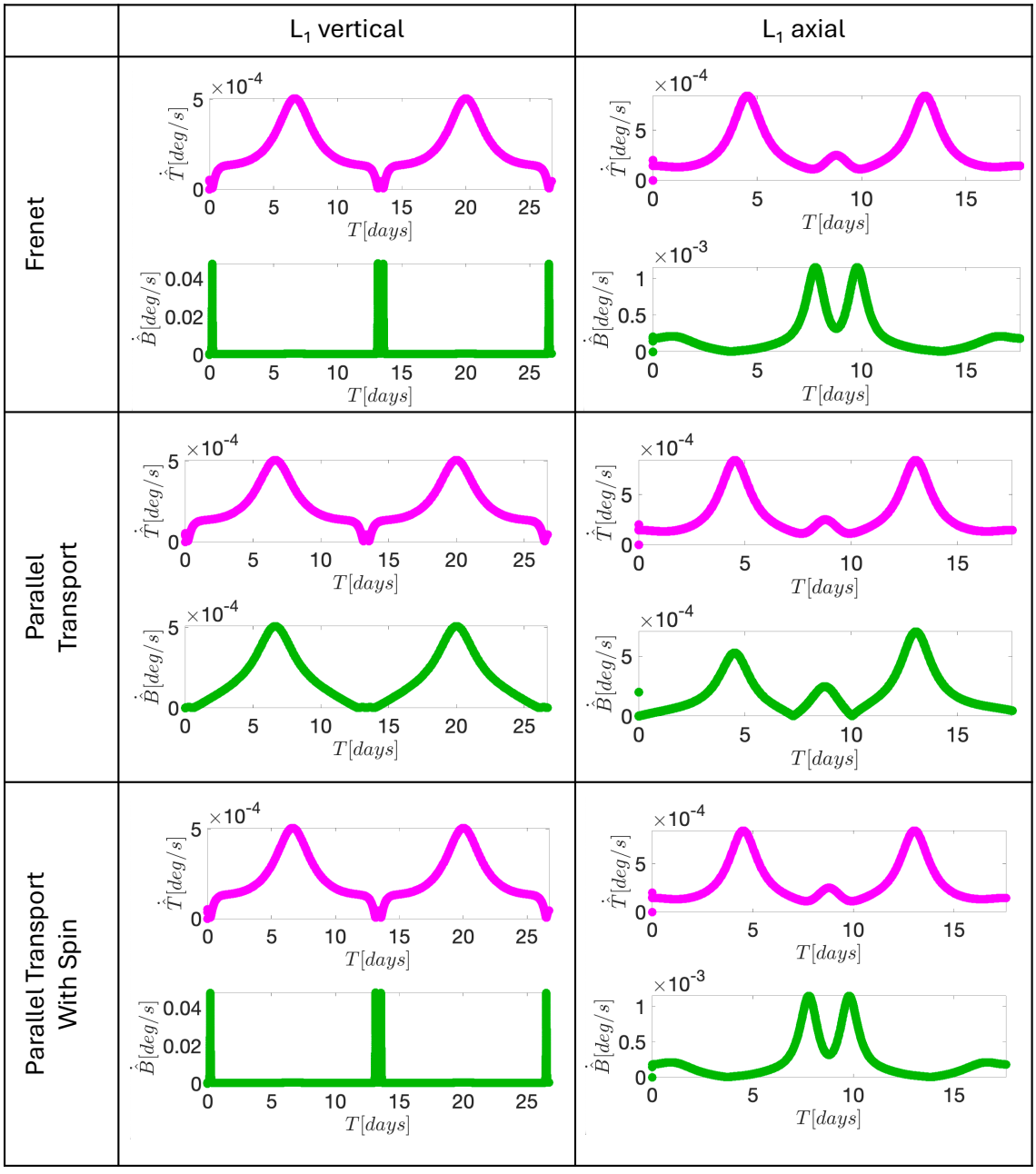

Figure 4. Discretely approximated time rate of change for each axis in each frame along two spatial orbits.

using the initial state, initial axes, time past the initial state, and angular velocity governing the axis evolution. As a result, these axes are uniquely defined. However, this definition could require flipping the components of a maneuver specified at the same location but separated by one period in these axes. For all three axes, the time rate of change of the angle between these axes produces values on the order of $10^{-4} - 10^{-3}$ deg/s.

Spatial General Trajectory

The final interesting example is a general spatial trajectory with a complex geometry. This trajectory performs a revolution near L_1, followed by a few revolutions around the Moon, before departing through the L_1 gateway into the Earth vicinity. For this trajectory, the axes at selected locations are plotted in Figure 5. Then, Figure 6 displays the angular difference between the two parallel trans-

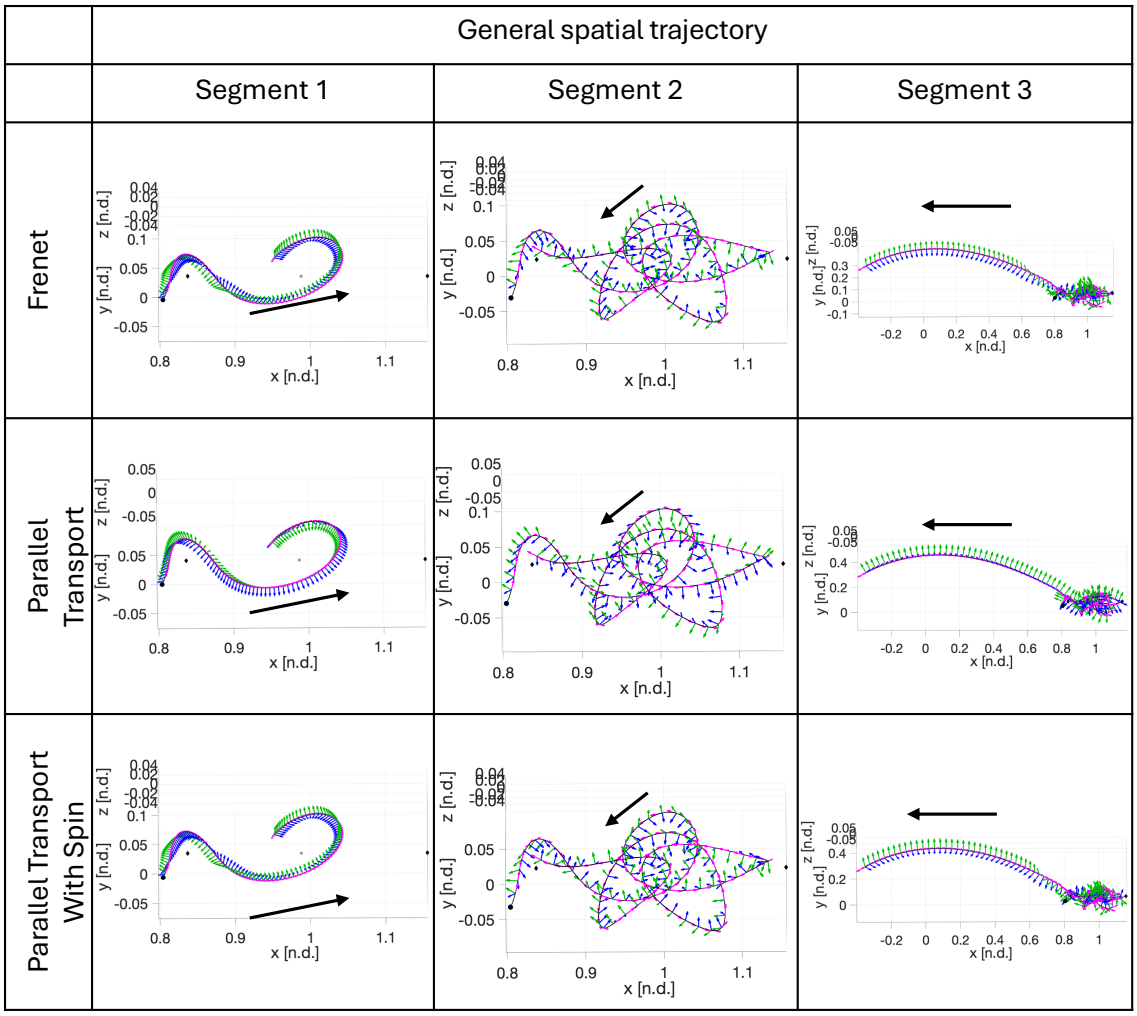

Figure 5. Examples of basis vectors computed along a general trajectory passing through various regions of the system using three distinct approaches. Basis vectors are colored as: tangent (magenta) and two vectors normal to tangent (green and blue). In the Frenet axes, green indicates the normal vector $\hat{N}_F$ and blue indicates the binormal vector $\hat{B}_F$.

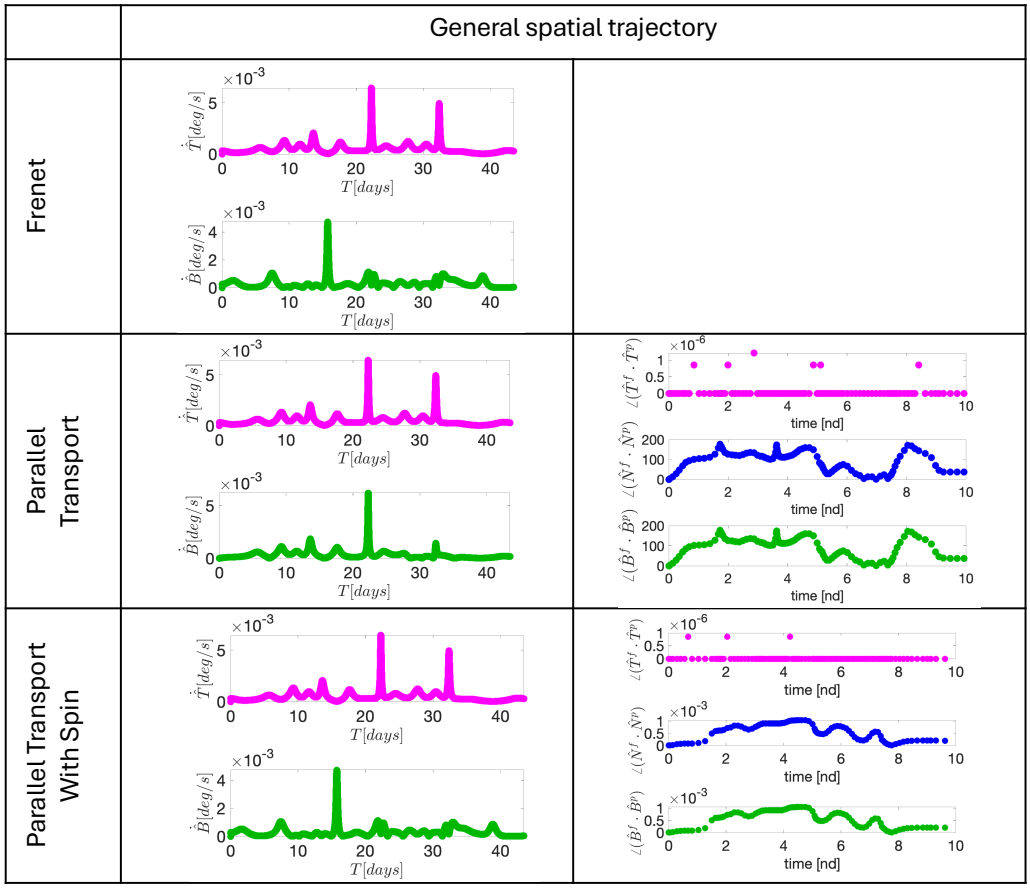

Figure 6. Comparison between the directions of the basis vectors computed in each parallel transport approach and the Frenet axes as well as discretely approximated time rate of change of basis vectors for the general trajectory.

port axes and the Frenet axes as well as the approximate time rate of change for the $\hat{T}$ and one vector that is calculated using the binormal vector $\hat{B}_F$ from the Frenet frame. In this example, the Frenet axes and parallel transport axes with additional spin due to torsion produce similar results. The axes in both cases evolve substantially along the trajectory, with some large direction changes occurring typically in regions where the spacecraft is moving slower. Furthermore, the binormal $\hat{B}_F$ and $\hat{M}_{2,R}$ vectors consistently capture the direction of motion of the spacecraft relative to the instantaneous center of curvature. However, the time rate of change of these axes reaches up to the order of 10^{-3} deg/s. For the parallel transport axes with no additional modifications, the two vectors $\hat{M}_{1,R}$ and $\hat{M}_{2,R}$ vary substantially from the Frenet axes, offering smoothly varying directions but less connection to geometric characteristics that provide maneuvering heuristics. Nevertheless, these axes can be calculated at any location along the trajectory, even in regions of low or zero curvature.

CONCLUSIONS

This paper explored curve-based frames as an analog to the well-known velocity-normal-conormal axes for specifying maneuvers for spacecraft operating in multi-body systems. The Frenet axes, defined in differential geometry to evolve with the curvature and torsion of a trajectory, captures meaningful information about the tangent to the path as well as two perpendicular vectors directed

within and normal to the osculating plane. Although these axes can support defining maneuvers using heuristics, they suffer from drastic changes in the orientation near regions of low curvature and can become undefined when the curvature is zero. A rotation-minimizing frame was also computed using a parallel transport approach. This frame begins with a selected set of axes, e.g., the Frenet frame, maintains the same tangent vector but only rotates the two remaining vectors enough to keep them normal to the tangent. As a result, the parallel transport axes produced smoothly varying basis vectors but at the expense of losing the geometric insight afforded by the Frenet frame. To capture the changing orientation of the osculating plane, a third definition uses the parallel transport approach but captures an additional spin around the tangent vector to mimic the torsion. In this case, the axes closely align with Frenet axes but also encounter a singularity when the curvature approaches zero. However, with further development, these curve-based axes may offer a useful analog to the velocity-normal-conormal axes that support maneuvering heuristics while being generalizable to diverse spacecraft trajectories that pass through various regions in a multi-body gravitational system.

ACKNOWLEDGMENT

This work was performed at the University of Colorado Boulder and supported by funding from the Air Force Research Laboratory through a cooperative agreement titled "Multi-Domain Awareness, Decision, and Exploitation". The authors also wish to acknowledge Maxwell Joyner's work in performing early analyses of rotation-minimizing frames using the double reflection method while funded by this project.

REFERENCES

[1] V. Szebehely, *Theory of Orbits: The Restricted Problem of Three Bodies*. London: Academic Press, 1967.

[2] W. S. Koon, M. W. Lo, J. E. Marsden, and S. D. Ross, *Dynamical Systems, the Three Body Problem and Space Mission Design*. New York: Marsden Books, 2011.

[3] K. Wardle, *Differential Geometry*. Mineola, NY: Dover Publications, Inc., 2008.

[4] N. Patrikalakis, T. Maekawa, and W. Cho, *Shape Interrogation for Computer Aided Design and Manufacturing*. Springer, Berlin, Heidelberg, 2009, E-book.

[5] F. Klok, "Two Moving Coordinate Frames for Sweeping Along a 3D Trajectory," *Computer Aided Geometric Design*, vol. 3, no. 3, pp. 217–229, 1986.

[6] W. Wang, B. Juttler, D. Zheng, and Y. Liu, "Computation of Rotation Minimizing Frames," *ACM Transactions on Graphics (TOG)*, vol. 27, no. 1, pp. 1–18, 2008.

[7] H. Guggenheimer, "Computing Frames Along a Trajectory," *Computer Aided Geometric Design*, vol. 6, no. 1, pp. 77–78, 1989.

[8] R. Bishop, "There is More than One Way to Frame a Curve," *The American Mathematical Monthly*, vol. 82, no. 3, pp. 246–251, 1975.

[9] A. J. Hanson and H. Ma, "Parallel Transport Approach To Curve Framing," *Indiana University, Techreports-TR425*, vol. 11, pp. 3–7, 1995.